Moscow University
Mathematics Bulletin
Vol. 58, No. 4, pp. 1–12, 2003

Vestnik Moskovskogo
Universiteta. Mekhanika
UDC 531.396

VESTIBULAR FUNCTION UNDER EXTREME CONDITIONS OF PERSONAL NAVIGATION AND ITS CORRECTION

V. A. Sadovnichii, V. V. Alexandrov, T. B. Alexandrova, S. S. Lemak, and A. M. Shkel

Operation of the human vestibular apparatus under extreme conditions does not provide full and reliable information for personal navigation. In this connection, there is a need to correct the vestibular function. In this paper we formulate a number of problems arising in this field of research. Extreme situations are described and their dynamic simulation is considered. Two kinds of corrections for the vestibular function are proposed.

1. EXTREME SITUATIONS AND OPERATION OF THE VESTIBULAR SENSORY APPARATUS

In the process of evolution of animal life, the vestibular apparatus was developed as a basic element of the animal's navigation system (in particular, of human personal navigation). Due to operation of this navigation system, an animal controls and stabilizes its movement [1].

The vestibular apparatus of a highly developed animal includes 1) three semicircular canals on each lateral side of its head (these canals form two near-orthogonal trihedrons) and 2) two pairs of otolithic organs (two utricles and two sacculi). Each canal can be represented as a thin curved duct of semicircular shape filled with endolymph (a viscous incompressible fluid).

Both ends of each duct are open and lowered into a reservoir (the utricle). One of these ends is sharply expanded in the immediate neighborhood of the utricle, forming an ampulla and narrowing down to the initial diameter.

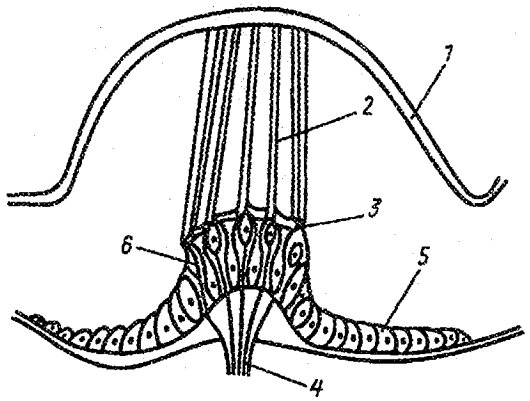

Fig. 1. The ampulla of the vestibular apparatus: *1* — the ampullary arch; *2* — the cupula; *3* — the subcupula area; *4* — the vestibular nerve; *5* — the supporting cells; *6* — the hair sensory cells

The cupula (an elastic jelly-like partition) resides inside the ampulla and is attached to the ampullary walls on the crista (a sensory base) in such a way that it is capable of deflecting in response to the motion of the endolymph (Figure 1). The crista contains hair sensory cells. The otolithic membrane is positioned inside the utricle. This membrane is of a complex shape, contains otoconial crystals and a jelly-like mass, and is able to displace along the macula (a sensory base of the utricle with hair sensory cells).

In contrast to the utricle, the sacculus is an almost isolated sac. The macula of the sacculus is situated on the vertical plane of the head. A displacement of the otolithic membrane inside the sacculus occurs along the macula [2].

In order to clarify the necessity of considering extreme situations during operation of the vestibular apparatus, below we present simplified mathematical models for the biomechanics of semicircular canals and otolithic organs.

As a mechano-theoretical model of semicircular canal dynamics, we consider the cupula as an elastic piston inside the ampulla under endolymph pressure (Figure 2). The endolymph is displaced relative to the walls of the canal in response to angular accelerations of the animal's head [3]. The following approximate mathematical model of cupula–piston dynamics is given in [3, 4]:

$$\ddot{x}_0 + \frac{8\nu}{a^2}\,\dot{x}_0 + \frac{\gamma}{m_0 k^4}\,x_0 = -\frac{R}{k^2}\left(1 + \frac{l}{\mathcal{L}}\right)\dot{\omega}. \tag{1}$$

Here x_0 is the linear displacement of the cupula–piston relative to its equilibrium position; $\dot{\omega}$ is the projection of angular acceleration (generated by rotation of the animal's head) onto the axis orthogonal to the semicircular canal plane; R is the outer radius of the canal; a is the inner radius of the canal; a_0 is the radius of the ampulla, $k = \dfrac{a_0}{a_1} > 1$ (Figure 2); $\mathcal{L}$ is the length of the canal; l is the length of the utricle, $l < \mathcal{L}$; $m_0 = \varrho\pi a^2\mathcal{L}$, where ϱ is the density of the endolymph; γ is the coefficient of elasticity of the cupula–piston; ν is the kinematic viscosity of the endolymph.

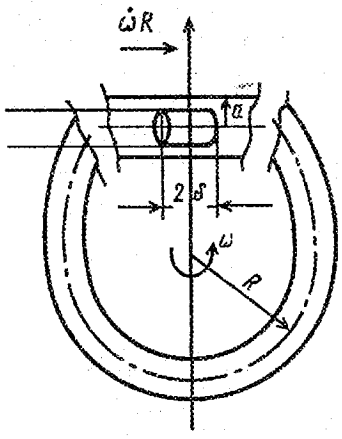

Fig. 2. The model of cupula–piston dynamics

Equation (1) was obtained by simplification of equations with small parameters describing the cupula–endolymph dynamics in the rotating semicircular canal. The possible endolymph leakage through the subcupula area is expressed by the coefficient $\dfrac{8\nu}{a^2}$ whose influence on the cupula dynamics is insignificant [3, 4]. If we assume that the cupula is a diaphragm completely blocking the ampullary cross section, then we obtain an equation similar to (1) with $\nu = 8\pi T$, where T is the stiffness of the diaphragm [4].

Let us consider the otolithic organ dynamics by the example of sacculi of fishes and amphibians. In this case, the otolithic membrane can be represented as a rigid body whose density ϱ_0 is several times greater than that of the endolymph surrounding the otolithic membrane in the sacculus [5]. We assume that the otolithic membrane is in plane-parallel motion along the local vertical plane of the sacculus under the action of the following forces:

— the gravitational force $\varrho_0 V_0 g$, where V_0 is the volume of the otolithic membrane and g is the gravitational acceleration;

— the endolymph buoyancy force $-\varrho V_0 g$ (the Archimedean force);

— the inertial forces $-m_2(w + \dot{\omega} \times r + \omega \times (\omega \times r) + 2\omega \times \dot{r})$, where $m_2 = (\varrho_0 - \varrho)V_0$, w is the absolute acceleration of the saccular reference point, ω is the absolute angular velocity of the animal's head, r is the vector of relative displacement of the center of mass for the otolithic membrane, and $r^{\top} = (x_1, x_2, 0)$;

— the viscous force $-\nu\dot{r}$ (the endolymph is a viscous fluid);

— the dynamic resistance force $-k_1\varrho\ddot{r}$ of the endolymph;

— the elastic force $-k_2 r$ due to the submembrane connected with the otolithic membrane (a columnar layer containing the cross-linked actinic filaments in contact with the microvilli of supporting cells [6]) and due to the hair bundles of sensory cells inside the saccular macula.

The equations describing the center-of-mass relative displacement of the otolithic membrane in the projections onto the macula axes of sensitivity Ox_1 and Ox_2 take the form

$$\frac{m_1}{m_2}\ddot{x}_1 + \frac{\nu}{m_2}\dot{x}_1 + \frac{k_2}{m_2}x_1 - \left(2\omega_3\dot{x}_2 + (\omega_3^2+\omega_2^2)x_1 + (\dot{\omega}_3 - \omega_1\omega_2)x_2\right) = g_1 - w_1, \tag{2}$$

$$\frac{m_1}{m_2}\ddot{x}_2 + \frac{\nu}{m_2}\dot{x}_2 + \frac{k_2}{m_2}x_2 + \left(2\omega_3\dot{x}_1 - (\omega_3^2+\omega_1^2)x_1 + (\dot{\omega}_3 - \omega_1\omega_2)x_1\right) = g_2 - w_2, \tag{3}$$

where $m_1 = (\varrho_0 + k_1\varrho)V_0$; $k_1\varrho V_0$ is the apparent additional mass of the otolithic membrane; g_1 and g_2 are the projections of the gravitational acceleration g; w_1 and w_2 are the projections of the absolute linear acceleration w; ω_1, ω_2, and ω_3 are the projections of the absolute angular velocity of the animal's head.

In the particular case of a single axis of sensitivity, the mathematical model (2), (3) coincides with that given in [7]. In order to describe the otolithic membrane dynamics of the mammalian sacculus or utricle, it is necessary to consider finite-dimensional models of large dimension (similar to (2) and (3)) or infinite-dimensional models [8]. Equations (2) and (3) model extreme situations adequately enough.

Thus, we may conclude that the canal–otolithic reaction (1)–(3) of the vestibular apparatus in response to mechanical stimuli is the reaction in response to the angular acceleration $\dot{\omega}$ of the animal's head and to the apparent acceleration $(w - g)$ of the reference point of the head. The normalized value

$$n = \frac{1}{g_0}(w - g) \tag{4}$$

is called the overload (here g_0 is the gravitational acceleration at the equator). The further evolution of this reaction (mechanoelectrical transduction, ion currents of hair cells in the crista and the macula, dynamics of neuromediator fluxes, appearance and propagation of afferent pulsations along nerve fibers) is discussed in [1, 4, 7]. In order to describe various extreme situations arising during operation of the vestibular apparatus, we first model the beginning of the canal–otolithic reaction (1)–(3). It should be noted that the dynamics of this beginning for the reaction (1) of the semicircular canal differs from that for the reaction (2), (3) of the otolithic organ. Dynamics of the cupula–piston (see (1)) or of the cupula–diaphragm corresponds to the dynamics of an overdamped torsion pendulum [1]. At the same time, the otolithic membrane dynamics (see (2), (3)) corresponds to that of a critically damped physical pendulum [7], which may give rise to eigenoscillations.

1.1. SENSORIAL CONFLICTS UNDER ZERO GRAVITY

Such an extreme situation can be observed, for example, during orbital flights. Under these conditions, the semicircular canal reaction in response to angular acceleration remains the same. However, it follows from (2) and (3) that the basic mechanical stimulus for the otolithic organ reaction is absent, since $(g - w) \sim 0$. Thus, the otolithic membrane dynamics under possible parametric disturbance $\omega(t)$ should be taken into account; in this case, the reactions of semicircular canals and otolithic organs become inconsistent, which causes vestibular disfunction [9, 10]. Many orbital experiments on fishes, amphibians, birds, and mammals were carried out in order to clarify the behavior of vestibular function in space. For example, a substantial proportion of experimental time (about 70 %) was given to such studies with biosatellites "Cosmos". The astronaut's vestibular function was studied on the orbital station "Mir" during 15 years of its operation. These experiments have provided a considerable amount of information on neuronal reactions of the vestibular apparatus in response to canal and otolithic stimulations under zero gravity [11] and on vestibular oculomotor reactions causing an increase in delay of eye fixation [12] (in a number of cases, this delay was responsible for emergency during visual control of spacecrafts). It should be noted that the variable delay in eye stabilization is of a chronic nature and continues after the astronaut's return to the Earth during the whole period of readaptation [12].

1.2. DISORIENTATION IN FLIGHT UNDER LARGE OVERLOADS

Any flight with large overloads ($|n(t)| > 1$) is characterized by various illusions (in particular, by appearance of false horizon and subjective vertical [13]). Large (up to $15\,g$) and fast varying overloads cause intensive reactions of semicircular canals in response to angular acceleration, which may lead to the astronaut's disorientation and emergency in space flights. Under these extreme conditions, the vestibular apparatus operates on the verge of its capabilities and the blood supply in the vestibular oculomotor apparatus is disturbed, which may lead to temporal loss in vision and, as a consequence, to disturbances in personal navigation and manual control.

1.3. SPACE MOTION SICKNESS, OR SEASICKNESS

Such an extreme situation can be observed in the case of steady roll of a ship or when moving by car along a road with complex profile or with many turns [14]. Most likely, this discomfort is caused by parametric disturbances of otolithic organ dynamics. It follows from (2) and (3) that when eigenoscillations of the otolithic membrane exist, the parametric resonance (undamped amplitudes) may appear under a certain combination of angular velocity frequencies and apparent acceleration frequencies. When a limit cycle is observed in the sensory cell dynamics [15], we may speak of the parametric resonance of a self-oscillating system.

1.4. LOSS OF THE VERTICAL POSE ON THE EARTH

Let us assume that the angle $\varphi(t)$ describes a loss of the vertical pose of a human being, $\varphi(t_0) = 0$ corresponds to the beginning of a fall, and $\varphi(t_1) = \frac{\pi}{2}$ corresponds to the end of a fall ($t_1 - t_0 \approx 1\ s$). Such a simplified model for the beginning of the canal–otolithic reaction (1)–(3) is described by the equations

$$\ddot{x}_0 + \frac{8\nu}{a^2}\,\dot{x}_0 + \frac{\gamma_0}{m_0 k^4}\,x_0 = -\frac{R}{k^2}\left(1 + \frac{l}{L}\right)\ddot{\varphi}(t),$$

$$\frac{m_1}{m_2}\,\ddot{x}_1 + \frac{\nu}{m_2}\,\dot{x}_1 - 2\dot{\varphi}(t)x_2 + \left(\frac{k_2}{m_2} - \dot{\varphi}^2(t)\right)x_1 - \ddot{\varphi}(t)x_2 = g_0 \sin\varphi(t) + \ddot{\varphi}(t)l,$$

$$\frac{m_1}{m_2}\,\ddot{x}_2 + \frac{\nu}{m_2}\,\dot{x}_2 + 2\dot{\varphi}(t)x_1 + \left(\frac{k_2}{m_2} - \dot{\varphi}^2(t)\right)x_2 - \ddot{\varphi}(t)x_1 = g_0 \cos\varphi(t) - \dot{\varphi}^2(t)l.$$

It follows from these equations that the canal–otolithic reaction in response to the mechanical stimulus $\varphi(t)$ ($t \in [t_0, t_1]$, rotation in the gravitational field) evolves as a complex movement of the cupula and the otolithic membrane. If for some reasons an adequate variation in conductance of transduction current is absent, then we may observe a delay in the information process of transmitting this reaction by afferent pulsations. As a result, vertical position stabilization may become impossible and its loss occurs.

2. DYNAMIC SIMULATION OF EXTREME SITUATIONS AND CORRECTION OF VESTIBULAR FUNCTION

In order to study the vestibular function in extreme situations, early in the XXth century several special dynamic stands were developed; animals or specimens of the vestibular system were placed on these stands.

Kinematic schemes of such stands are different: rotary tables, dynamic platforms, support-type stands, centrifuges with or without gimbals, etc. In 1903, Tsiolkovsky carried out first experiments with insects in centrifuges in order to clarify their abilities to endure large overloads. In the 1920s, B. and Ch. Diringshefens and G. Stike [17] initiated the formation of experimental centers to study the influence of various flight factors on humans. Gradually, centrifuges with gimbals have gained wide acceptance among different dynamic stands [16].

2.1. A KINEMATIC SCHEME OF CENTRIFUGES WITH CONTROLLABLE GIMBALS

Let us consider a centrifuge with a cabin in the gimbal (Figure 3). The console of the centrifuge is capable of rotating in a horizontal plane with angular velocity $\omega_k(t)$. The gimbal is attached to the end of the console. The hemisphere of the gimbal (fork, Figure 3) has the axis of symmetry coincident with the console and is able to rotate through the command angle φ. The axis of the inner ring is fixed in its initial vertical position inside the outer ring (the boundary of the hemisphere); the inner ring is capable of rotating about this axis through the command angle ψ. The axis of the cabin (capable of rotating through the command angle γ) is fixed in the inner ring and is perpendicular to the axis of this ring. Thus, the above dynamic stand is a control mechanical system with four degrees of freedom. Let us consider the question of how to use such a stand to simulate extreme conditions.

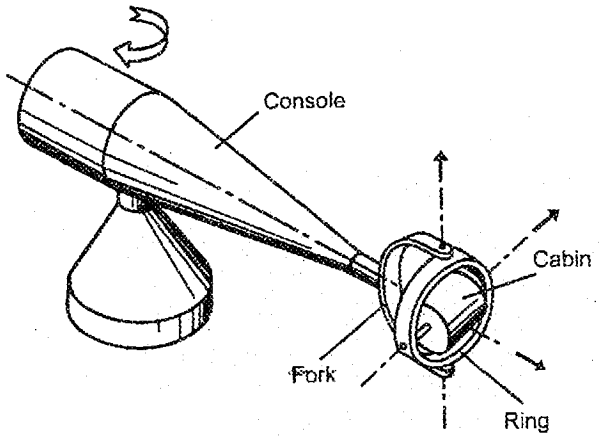

Fig. 3. A centrifuge with the controllable gimbal

2.2. SIMULATION OF APPARENT ACCELERATION (OF THE OVERLOAD VECTOR n)

Let us assume that the axis of rotation of the inner ring is initially vertical and the axis of rotation of the cabin is horizontal and is directed perpendicularly to the console. The fixed coordinate frame $O'\xi\eta\zeta$ is associated with the axis of rotation of the centrifuge ($O'\xi$-axis is vertical). The coordinate frame $O'XYZ$ is rigidly associated with the console; the $O'X$-axis coincides with the $O'\xi$-axis and the $O'Y$-axis is directed along the console. The axes of the coordinate frame $OXYZ$ with its origin at the center of the gimbal are parallel to the axes of the coordinate frame $O'XYZ$. The coordinate frames $Ox_1y_1z_1$, $Ox_2y_2z_2$, and $Oxyz$ are rigidly associated with the fork, the inner ring, and the cabin, respectively. The transition from the coordinate frame $O'XYZ$ to the coordinate frame $Oxyz$ can be represented as follows:

$$XYZ \;\frac{\theta}{Y, y_1}\; x_1y_1z_1 \;\frac{\psi}{x_1, x_2}\; x_2y_2z_2 \;\frac{\gamma}{z_2, z}\; xyz.$$

Here the angles of rotation θ and ψ are introduced in a clockwise direction, whereas the angle γ is introduced in a counterclockwise direction. The overload (4) formed by the centrifuge is equal to $n^T = (n_X, n_Y, n_Z) = \left(1, -\dfrac{\omega^2 l}{g}, \dfrac{\dot{\omega} l}{g}\right)$, where n_X, n_Y, and n_Z are its projections onto the axes of the coordinate frame $OXYZ$, l is the length of the console, and ω is the rate of rotation of the console about the $O'\xi$-axis.

The projections of the overload vector $n^0(t)$ onto the axes of the coordinate frame associated with the cabin are known as time functions. In the process of simulation, it is necessary to choose the angles of the gimbal and the rate of rotation of the console in such a way that the inequality $\|n - n^0(t)\| < \varepsilon$ be valid (here ε is an accuracy of simulation [18]).

The algorithm for simulation of overloads can be divided into two steps. First, the required rate of rotation of the console is determined from the solution of the problem on simulation of the overload vector

magnitude. Second, the angles of rotation made by the rings of the gimbal are determined from the solution of the problem on simulation of the overload vector direction.

Dynamic simulation of the overload vector magnitude. This magnitude satisfies the equality

$$|n|^2 = n^2 = 1 + \frac{\omega^4 l^2}{g^2} + \frac{\dot{\omega}^2 l^2}{g^2}.$$

From here we can obtain the following equation for the required angular velocity of the centrifuge:

$$\dot{\omega}^2 + \omega^4 = \left(\frac{g}{l}\right)^2 \left(n^2 - 1\right). \tag{5}$$

Note that under terrestrial conditions it is impossible, using a centrifuge, to simulate an overload whose magnitude $|n(t)|$ is less than 1. In this case, it is possible to simulate only the direction of the overload vector when the console does not rotate. Equation (5) is not expressed in terms of the higher derivative. It is well known [16] that when its right-hand side is quasistationary, it is possible to construct a piecewise differentiable solution to equation (5).

We solve equation (5) by a finite-difference scheme as follows. Let a uniform time grid t_k with a simulation step $\tau = t_{k+1} - t_k$ $(k = 0, 1, \ldots)$ be given. It is assumed that for any t_k the value $c_{k+1} = c(t_{k+1})$ is known (here $c(t) = \frac{g}{l}\sqrt{n^2(t) - 1}$). In order to find $\omega(t)$ on the segment $[t_k, t_{k+1}]$, we use the following approximation:

$$\omega(t) = \sqrt{\omega^2(t_k) + U_k(t - t_k)}.$$

This approximation is most simple, since it is linear with respect to $W = \omega^2$:

$$W(t) = W_k + U_k(t - t_k).$$

Now we choose U_k in such a way that for any $[t_k - 0]$ the equality (5) be fulfilled. When $\omega^2 = W$, this equality takes the form $U_k^2 + 4W^3 = 4Wc^2$. At the instant t_{k+1}, equation (5) can be rewritten as

$$U_k^2 + 4W_{k+1}^3 = 4W_{k+1}c_{k+1}^2. \tag{6}$$

The following two cases are possible.

A) The case $W_k \le c_{k+1}$. This means that the overload increases and remains constant. Let $x = W_{k+1}$; then $U_k = \frac{1}{\tau}(x - W_k)$, where x is a root of $F(x) = 0$ for $\tau = t_{k+1} - t_k$:

$$F(x) = 4\tau^2 x^3 + x^2 - 2\left(W_k + 2\tau^2 c_{k+1}^2\right)x + W_k^2. \tag{7}$$

This equation is obtained from (6) by substitution $U_k = \frac{1}{\tau}(x - W_k)$. Note that we are interested only in nonnegative roots of $F(x) = 0$, since $\omega_{k+1}^2 = W_{k+1} = x$. When $W_k = 0$, equation (7) takes the form

$$x\left(4\tau^2 x^2 + x - 4\tau^2 c_{k+1}^2\right) = 0.$$

Hence, its nonnegative solution is

$$x = \frac{-1 + \sqrt{1 + 64\tau^4 c_{k+1}^2}}{8\tau^2} \ge 0.$$

If $W_k > 0$, then we seek a root of $F(x) = 0$ on the segment $[W_k, c_{k+1}]$. Such a root always exists, since $F(W_k) \le 0$ and $F(c_{k+1}) \ge 0$.

B) The case $c_{k+1} < W_k$. This means that the overload decreases. The function $F(x)$ is a third-degree polynomial with a single negative root. Hence, on the positive semiaxis the minimum is attained at the point

$$x_0 = \frac{\sqrt{1 + 24\tau^2\left(W_k + 2\tau^2 c_{k+1}^2\right)} - 1}{12\tau^2}.$$

If at this point we have $F(x_0) \le 0$, then a solution (one or two) exists; a value of W_{k+1} should be chosen from the segment $[x_0, W_k]$.

When $F(x_0) > 0$, there exists no solution to (7); therefore, W_{k+1} should be set equal to that value of x_0 where $F(x)$ attains its minimum. The above algorithm allows us to find the required angular velocity of the centrifuge in real time mode.

Simulation of the overload vector direction. Let an angular velocity of the console be chosen. Now we find the angles of rotation for the gimbal. These angles allow us to orient the vector $n^0(t)$ in the coordinate frame associated with the cabin.

The projections of the overload vector take the following form at the center of the gimbal in the coordinate frame $Oxyz$ rigidly associated with the cabin:

$$\begin{aligned} n_x &= \cos\theta\cos\gamma + \sin\theta\sin\psi\sin\gamma - \frac{\omega^2 l}{g}\cos\psi\sin\gamma + \frac{\dot\omega l}{g}(\sin\theta\cos\gamma - \cos\theta\sin\psi\sin\gamma), \\ n_y &= -\cos\theta\sin\gamma + \sin\theta\sin\psi\cos\gamma - \frac{\omega^2 l}{g}\cos\psi\cos\gamma + \frac{\dot\omega l}{g}(-\sin\theta\sin\gamma - \cos\theta\sin\psi\cos\gamma), \\ n_z &= -\sin\theta\cos\psi - \frac{\omega^2 l}{g}\sin\psi + \frac{\dot\omega l}{g}\cos\theta\cos\psi. \end{aligned} \tag{8}$$

Note that the equalities (8) are not independent: in order to orient the overload vector, it is sufficient to perform two rotations of the gimbal. For example, we may simulate the overloads by fixing the "fork" and by finding the required angles of rotations for the ring and the cabin from (8).

In many cases, however, such an approach leads to very large variations in angles of rotation at each step of simulation; this requires large angular accelerations for the ring and the cabin, which may distort the pattern of canal–otolithic reactions in the vestibular system.

In order to reduce the influence of spurious angular accelerations, it is reasonable to use all the three angles of rotation of the gimbal and to minimize the sum angle at each step of simulation. For each t_k $(k = 1, 2, \ldots)$, the required angles of rotation can be found from the following minimization problem:

$$J(\theta_k) = (\theta_k - \theta_{k-1})^2 + (\psi_k - \psi_{k-1})^2 + (\gamma_k - \gamma_{k-1})^2 \longrightarrow \min_{\theta_k \in [-\pi,\pi]}. \tag{9}$$

Here $\psi_k = \psi_k(\theta_k)$ and $\gamma_k = \gamma_k(\theta_k)$.

If θ_k is fixed, then from (8) we can find the explicit expression for ψ_k:

$$\psi_k = \arcsin\frac{n_y}{\sqrt{s_1^2 + s_3^2}} + arctan\frac{s_3}{s_1}. \tag{10}$$

Here $s_1 = \dfrac{l\omega^2}{g}$ and $s_3 = \dfrac{l\dot\omega}{g}$. Knowing ψ_k, we find γ_k:

$$\gamma_k = arctan(s_2) - \arcsin\frac{n_z}{\sqrt{1 + s_2^2}}. \tag{11}$$

Here $s_2 = s_3\sin\psi_k - s_1\cos\psi_k$.

Note that (9) is a problem of one-dimensional constrained minimization for a nonlinear function. Its solution can be obtained with an adequate accuracy by the algorithm of finding global extrema given in [19].

2.3. TRAINING ON SIMULATION STANDS AND CORRECTIONS OF VESTIBULAR FUNCTION

In Section 1 of this paper we have described the extreme situations for personal navigation when operation of the vestibular apparatus should be corrected. Two kinds of corrections for the vestibular function and two kinds of help for the vestibular apparatus are possible.

First, training helps a human being in faster adaptation to an extreme situation and in correction of information coming from the vestibular system (in other words, training helps in the formation of conditioned reflexes).

Second, vestibular prostheses help in the correction of vestibular function up to the complete replacement of this function when the vestibular apparatus does not work. Pharmacological remedies for such corrections and replacements are not discussed here.

Let us consider the first kind of corrections. It is clear that the correction training should be performed on dynamic stands; this allows one to simulate extreme situations dynamically. It was shown in Subsection 2.2 of this paper that the apparent acceleration (a basic mechanical stimulus for otolithic organs) can be simulated dynamically and that centrifuges with controllable gimbals are most reasonable. Generally, however, angular velocities of simulating motion may not correspond to those of actual motion. In the case of quasisteady simulating motion, according to [17, 18], this inconsistency is not essential. This allows us to propose an algorithm for dynamic simulation of controllable reentry from an orbit [16] and to train astronauts for the International Space Station at the Gagarin Training Center.

The problem of dynamic simulation can be considered in the following more complex formulation: it is required to find simulating motions such that the mechanical stimuli for the canal–otolithic system and the dynamics of canal–otolithic reactions on a stand be similar to those for actual motions.

For the above kind of corrections, another problem would require its formulation and solution. It is necessary to correct the vestibular function in order to refine navigational information and to improve the control of human motion or the motion of an object. Therefore, the scope and duration of preflight training should be specified on the basis of quality testing of required experience in space control. One of the approaches to guaranteed testing is discussed in [20, 21].

3. CORRECTION OF VESTIBULAR FUNCTION BY MICRO-ELECTRO-MECHANICAL SYSTEMS

3.1. MEMS-BASED TECHNOLOGY AND MICROGYROSCOPES

The principal use of gyroscopes is to measure orientation, heading, or pointing direction. By now, many different gyroscope concepts have been developed: from high-end inertial navigation instruments to low-end consumer product sensors [22]. This diversity in performance and operational requirements has spawned a vast diversity in gyroscope technology: for example, spinning wheel, vibrating tuning fork, solid-state laser, and magnetohydrodynamic gyroscopes. Almost all the high-end precision technologies are characterized by high cost, large sizes, and appreciable power consumption; at the same time, the use of micromachining technology allows one to design inexpensive miniature gyroscopes with good performance [22].

Mechanical microgyroscopes are emerging from the technology developed for integrated circuits (IC). The recent advance in computer processor technology has led to a considerable demand for small systems or Micro-Electro-Mechanical Systems (MEMS) that can fully exploit the benefits of IC microtechnology. The IC industry's ability to deposit and etch the micron-scale features in silicon and aluminum has been exploited to build tiny inertial sensors. The compatibility of MEMS and IC allows the integration of mechanical structures alongside microcircuits on one and the same chip. These studies are successfully conducting at the University of California, USA [22, 23].

Placing interface electronics, signal processing circuits, and analog-to-digital conversion on a chip results in improved noise performance, extreme miniaturization, and inexpensive manufacturing. The need for a multitude of discrete components on large printed circuit boards is virtually eliminated. Potentially, a device that is able to accurately sense, extract, and transmit three-dimensional motion can be built on a single silicon chip and fit in a volume smaller than one cubic centimeter.

A prototype of the semicircular canal prosthesis was designed due to the MEMS-based technology. The purpose of such a prosthesis is to restore the balance function. Ideally, the prosthesis will be able to sense motion with sufficient precision and to deliver signals to the central neural system, matching the signals that the natural organ would generate.

The classical micromachined gyroscope is composed of a spinning wheel or rotor which exhibits Coriolis acceleration when an object rotates due to conservation of angular momentum. Unfortunately, the scaling laws do not allow one to fabricate microgyroscopes operating on rotational principle (due to unfavorable scaling of friction and significant decrease in mass). In recent years, several new approaches were proposed to design and build gyroscopes which are microscopic in size and are able to sense angular rotation using vibrational elements [23, 24].

In the vibratory gyroscopes based on this principle, the structure is driven into resonance and the rotation-induced Coriolis force causes the transfer of energy from the driven vibrational mode to a sense vibrational mode. The magnitude of energy transferred is proportional to the rate of rotation. An ensemble

of six inertial MEMS sensors integrated on a single silicon chip is required to measure six degrees of freedom of the head motion [25].

Our first prototype of the vestibular prosthesis is implemented using polysilicon surface micromachining technology. In the prosthesis, the three semicircular canals are replaced by three-axes MEMS gyroscopes, while the two otolith organs are replaced by three-axes accelerometers. The MEMS accelerometer consists of a proof mass suspended by compliant beams anchored to a fixed frame.

External acceleration (due to motion of the object to which the sensor's frame is attached) displaces the support frame relative to the proof mass, which in turn, changes the initial stress in the suspension spring. Both this relative displacement and the suspension-beam stress can be used as a measure of the external (apparent) acceleration (4).

In the most general case, the proof-mass motion can have six degrees of freedom. Typically, however, in a unidirectional accelerometer, the geometrical design of the suspension is such that one of these axes has low stiffness while high stiffness along other axes. In the case of the z-axis accelerometer, for example, the proof mass of the device will displace in out-of-plane of the chip only if there is an acceleration component along the z-axis.

Our micromachined gyroscopes use a vibrating element to measure the rotational velocity on the basis of the Coriolis principle [26].

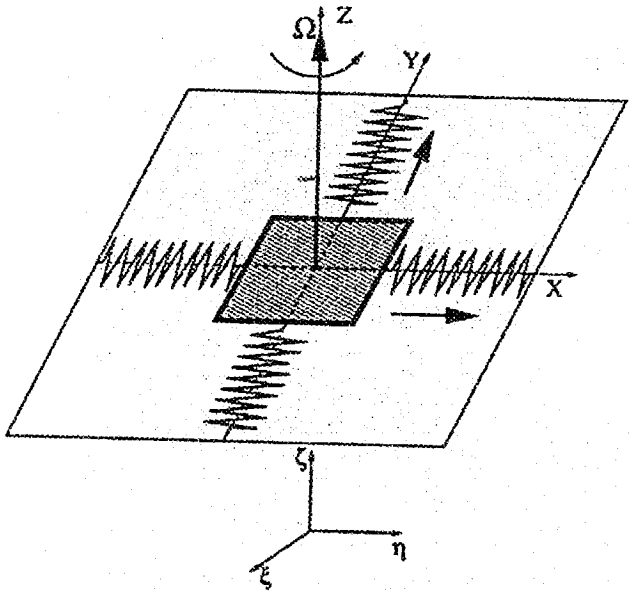

Fig. 4. The model of a vibratory gyroscope

Just like a linear accelerometer, the micromachined vibrating angular-rate sensor consists of the proof mass on an elastic suspension. This configuration allows two-degrees-of-freedom motion of the mass. In the basis of operation, the proof mass (which constitutes the active portion of the sensor) is driven by an oscillator circuit at a constant amplitude and high frequency. When subjected to a rotation, the proof mass will be subjected to the Coriolis force $F = 2m\Omega \times V_c$ (here m is the mass, V_c is the instantaneous radial velocity of the center of mass, and Ω is the input rate of rotation). As an illustrative example, let us consider a z-axis gyroscope (sensing the rotation with respect to the z-axis, i.e., the axis perpendicular to the chip). The equations of proof-mass motion are naturally described with respect to the noninertial coordinate frame $\{x, y, z\}$ (Figure 4). In this case, the simplified equations in Cartesian coordinates $\{x, y, z\}$ take the form

$$\ddot{x} + \omega_n^2 x - 2\Omega\dot{y} = 0,$$
$$\ddot{y} + \omega_n^2 y + 2\Omega\dot{x} = 0.$$

The essential feature of these equations is the presence of the Coriolis acceleration terms $-2\Omega\dot{y}$ and $2\Omega\dot{x}$. It is the Coriolis acceleration that causes a transfer of energy between the two gyroscope modes of operation.

The resultant Coriolis force is perpendicular to both the input rate of rotation and the instantaneous radial velocity in the drive direction. This produces a motion of the proof mass in the direction perpendicular to its initial oscillation (i.e., in the sense direction).

In order to measure the rate of rotation, the proof mass is driven to a fixed amplitude along the x-axis by applying an electrostatic drive force to the proof mass along the x-axis. In the absence of rotation there will be no motion of the proof mass along the y-axis (Figure 4). Under rotation, however, the Coriolis acceleration will cause energy to be transferred from the x-axis (primary mode) to the y-axis (the axis of sensitivity, secondary mode) building up a vibration amplitude along the y-axis. The ratio of the amplitude in the secondary mode of vibration to the amplitude of the primary mode of vibration can be shown to be proportional to the rotation rate and is given by $\frac{y}{x} = 2Q\frac{\Omega}{\omega_n}$. Note that the gyroscope response is proportional to the quality factor Q of the device (in other words, is inversely proportional to the losses of energy). Therefore, the design objective is to maximize the amplitude of response in the sense direction by maximizing the quality factor Q. This can be achieved, for example, by vacuum packaging the MEMS gyroscopes and thus decreasing gas damping within the chip's cavity.

In the case of the x-axis gyroscope, the proof mass is driven to a fixed amplitude along the y-axis by applying an electrostatic drive force to the proof mass along the y-axis. Under rotation with respect to the x-axis, the Coriolis acceleration will cause energy to be transferred from the y-axis (primary mode) to the z-axis (secondary mode) building up a vibration amplitude perpendicular to the surface of the chip. The amplitude is measured and related to the input angular velocity along the x-axis. Measurements along other axes are performed in a similar way.

The above-described principle of operation is not the only option for implementation of MEMS gyroscopes. Multidegree-of-freedom gyroscopes and vibratory gyroscopes capable of measuring the angle of rotation directly are also proposed [22].

Thus, the sensing unit of the proposed vestibular prosthesis should include three-axes accelerometers and three-axes gyroscopes implemented on the same silicon chip. Technologically, this goal can be achieved. The above-described configuration of microdevices allows us to measure all six-degrees-of-freedom motions of the human head. The output signals from the accelerometers and gyroscopes are voltages proportional to linear accelerations and angular velocities, respectively. The rotational perceptual threshold in humans was determined to be between 0.1 and 2 grad/s^2 [27]. It should be noted, however, that perceptual thresholds are different for different rates of acceleration and vary from person to person. Montandon [28] determined that the threshold is 1 grad/s^2 in healthy individuals, but greater than 6–7 grad/s^2 in patients with vestibular disfunction. The reported sensation limits set the sensitivity requirements for the vestibular prosthesis. Our results and results of other groups working on MEMS inertial sensors demonstrated that the required performance level is readily achievable [22].

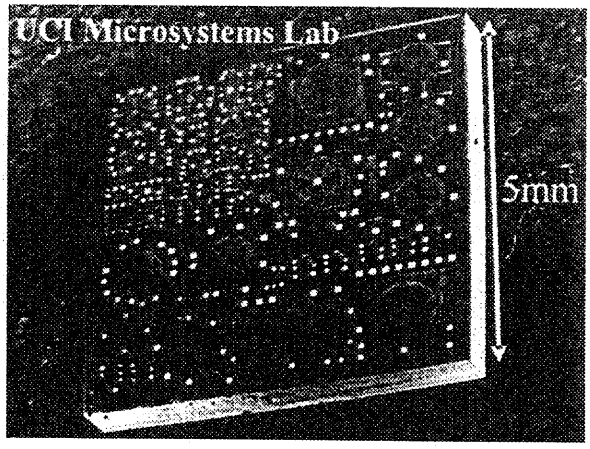

Fig. 5. The prototype of the vestibular prosthesis

The gyroscope is able to sense any type of angular rotation (constant or nonconstant angular velocities), while the natural vestibular organ is only responding to the angular acceleration. In order to mimic the natural organ, therefore, the supporting circuit electronically differentiates the output voltage from the

gyroscope to produce a signal proportional to the angular acceleration. In our prototype (Figure 5), the circuit uses a low-pass filter before the differentiator for minimizing the effect of high-frequency noise [29].

3.2. ARCHITECTURE OF THE VESTIBULAR PROSTHESIS

The vestibular prosthesis includes three main functional units (a sensing unit, a pulse generator, and a stimulator) and two supporting units (a power supply, an external controller, and a charging unit) [30].

The sensing unit comprises three-axes accelerometers and three-axes gyroscopes. These devices sense linear and angular motion of the head and generate voltages proportional to the corresponding linear acceleration and angular velocity. Then, these voltages are sent to the pulse generator where angular velocities (or linear accelerations) are translated into voltage pulses. In the stimulator, the voltage pulses are converted into current pulses and are delivered transcutaneously by small-amplitude galvanic current to the vestibular afferents that lie directly below the mastoid bones. Each functional block of the chip consumes electrical power. For long-term autonomous operation of the prosthesis, it is required to supply power externally. Hence, the prosthesis should be able to communicate with an external controller and a charging unit.

The work was supported by the Russian Foundation for Basic Research (01–01–00415) and by UC MEXUS-CONACYT (CN–02–70).

REFERENCES

1. I.V. Orlov, *Vestibular Function* (in Russian), St. Petersburg, 1998.
2. A.A. Shipov, A.V. Kondrachuk, and S.P. Sirenko, *Biomechanics of the Vestibular Apparatus* (in Russian), Moscow, 1997.
3. T.G. Astakhova, "A mathematical model for a semicircular canal of the vestibular system as an angular acceleration sensor", *Vestn. Mosk. Univ. Matem. Mekhan.*, 1: 69–72, 1989.
4. V.A. Sadovnichii, V.V. Alexandrov, T.B. Alexandrova, A. Almanza, T.G. Astakhova, R. Vega, N.V. Kulikovskaya, E. Soto, and N.E. Shulenina, "A mathematical model for the mechanoreceptor of angular accelerations", *Vestn. Mosk. Univ. Matem. Mekhan.*, 6: 46–55, 2002.
5. D.V. Lychakov, "Evolution of otolithic membranes", *Zhurn. Evolutsionnoy Biokhim. i Fiziol.*, **XXIV**, 2: 250–266, 2002.
6. B. Kachar, M. Parakkac, and J. Fex, "Structural basis for mechanical transduction in the frog vestibular sensory apparatus. I: The otolithic membrane", *H. Res.*, **45**: 179–190, 1990.
7. J.M. Goldberg and C. Fernandes, "Vestibular mechanisms", *Annu. Rev. Physiol.*, **37**: 129–162, 1975.
8. A.V. Kondrachuk, "Modeling of structure and mechanics of otolithic membranes", *Aviakosm. i Ekologich. Meditsina*, **34**, 5: 45–51, 2000.
9. L. Kornilova, L. Jakovleva, N. Tarasov, and G. Gorgiladze, "Cosmonaut's vestibular disfunction during microgravitation adaptation and readaptation", *Physiologist*, **20**: 535–536, 1983.
10. D.E. Parker, M.F. Resenke, A.P. Arrott, J.L. Homick, and B.K. Lichtenberg, "Otolith tilt-translation reinterpretation following prolonged weightlessness: implications for preflight training", *Aviat. Space and Environ. Med.*, **56**: 601–605, 1985.
11. I. Kozlovskaya, N. Sirota, B. Babaev, et. al., "Human and animal results on vestibular research in space", *The 4th European Symposium on Life Science Research in Space*, Trieste, 353–357, 1990.
12. M. Reschke, L. Kornilova, D. Harm, et. al., "Neurosensory and sensory-motor function", *Space Biology and Medicine, Joint US/Russian Publication. AIAA*, **3**, 1: 135–193, 1997.
13. R.A. Peters (Ed.), *Dynamics of the Vestibular System and its Relation to Motion Perception, Spatial Disorientation and Illusions*, NASA CR–1309.
14. K.L. Khilov, *The Function of Equilibrium Organs and Disturbances in Motion Perception* (in Russian), Leningrad, 1969.
15. M. Ospeck, V.M. Eguiluz, and M.O. Magnasco, "Evidence of Hopf bifurcation in frog hair cells", *Biophys. J.*, **80**: 2597–2607, 2001.
16. V.V. Alexandrov, L.I. Voronin, Yu.N. Glazkov, A.Yu. Ishlinsky, and V.A. Sadovnichii, *Mathematical Problems of Dynamic Simulation in Space Flights* (in Russian), Moscow, 1995.
17. G. Glaser, *Dramatische Medizin* (in German), Zürich, 1959.

18. V.V. Alexandrov, "Simulation of apparent accelerations", *Dokl. Akad. Nauk SSSR*, **256**, 2: 345–348, 1980.

19. R.G. Strongin, "Numerical methods in multiextremal problems (information-statistical algorithms)", in: *Optimization and Operations Research* (in Russian), Moscow, 1978.

20. V.V. Alexandrov, "Quality testing in stabilization of unsteady motions", *Vestn. Mosk. Univ. Matem. Mekhan.*, 3: 51–54, 1997.

21. V.V. Alexandrov, S.S. Lemak, and D. Vera Mendoza, "Accuracy testing in magnetic stabilization of small satellites", *Vestn. Mosk. Univ. Matem. Mekhan.*, 5: 66–73, 1999.

22. A. Shkel, "Micromachined gyroscopes: challenges, design solutions, and opportunities", *The 2001 SPIE Annual International Symposium on Smart Structures and Materials (Invited Paper)*, Newport Beach, 2001.

23. A.M. Shkel and R.T. Howe, *Micromachined Angle-Measuring Gyroscope*, U.S. Patent 6,481,285, Nov. 19, 2002.

24. C. Painter and A. Shkel, "Structural and thermal modeling of a z-axis rate integrating gyroscope", *J. Micromechanics and Microengineering. Institute of Physics Publishing*, **13**: 229–237, 2003.

25. A. Shkel, "Smart MEMS: micro-structures with error-suppression and self-calibration control capabilities", *The American Control Conference*, Arlington, 2001.

26. A. Shkel, A. Horowitz, A. Seshia, S. Park, and R. Howe, "Dynamics and control of micromachined gyroscopes", *The American Control Conference*, San Diego, 1999.

27. A. Benson, "Thresholds for the perception of whole body angular movement about a vertical axis", *Aviat. Space and Environ. Med.*, **60**: 205–213, 1989.

28. A. Montandon, "A new technique for vestibular investigation", *ACTA Otolaryngol.*, **39**: 594, 1954.

29. J. Liu, A. Shkel, K. Nie, and F. Zeng, "System design and experimental evaluation of a MEMS-based semicircular canal prosthesis", *Proc. Int. IEEE EMBS Conf. on Neural Engineering*, Capri Island, 2003.

30. A.M. Shkel, J. Liu, C. Ikei, and F.-G. Zeng, "Feasibility study on a prototype of vestibular implant using MEMS gyroscopes", *Proc. Int. IEEE Conf. on Sensors*, pp. 1526–1531, Orlando, 2002.

28 February 2003